Proceedings of the 5th International Symposium on Steel Science (ISSS 2017)
Nov. 13-16, 2017, Kyoto, Japan: The Iron and Steel Institute of Japan

Carbon partitioning during quenching and partitioning heat treatment

Yuki Toji[1*], Hiroshi Matsuda[1], Goro Miyamoto[2], Michael Herbig[3], Pyuck-Pa Choi[4], Dierk Raabe[3]

[1] Steel Research Laboratory, JFE Steel Corporation, 1 Kawasaki-cho, Chuo-ku, Chiba, 260-0835, Japan
[2] Tohoku University, 2-1-1 Katahira, Aoba-ku, Sendai, 980-8577, Japan
[3] Max-Planck-Institut für Eisenforschung GmbH, Max-Planck-Str. 1, Düsseldorf, 40237, Germany
[4] KAIST, 291 Daehak-ro, Yuseong-gu, Daejeon, 305-701, Korea

Abstract: Carbon partitioning from martensite into austenite in the quenching and partitioning (Q&P) process has been suggested to be controlled by the constrained carbon equilibrium (CCE) criterion. This predicts the austenite carbon concentration under the conditions that competing reactions such as bainite transformation and carbide formation are suppressed. However, such competing reactions have repeatedly been observed in the Q&P process. This study aims to reveal the complicated competing phenomena by separating each of them. 0.59 wt% carbon steel was austenitized, water-quenched and partitioned at 400 ˚C. 8 vol% austenite existed in the as-quenched specimen. X-ray diffraction confirmed that bainite transformation did not occur at 400 ˚C. Clear carbon enrichment in austenite was detected by atom probe tomography in the partitioned specimens. The results revealed carbon partitioning from martensite into austenite excluding any effects from bainite transformation. Carbon partitioning accompanied by carbide precipitation in martensite was investigated using 1.07 and 0.59 wt% carbon steels with various martensite volume fractions. Carbon partitioning was clearly observed in both steels even though considerable carbide precipitation was observed. The austenite carbon concentration after the partitioning step was not influenced by either martensite volume fraction or bulk carbon content, which is inconsistent with the CCE model. A modified prediction model, which can be applied to the case where carbide precipitation occurs in martensite, was proposed. The austenite carbon concentration predicted by the modified model showed the same trend as the experimental results, and was closer to the experimental value than that predicted by the original CCE model.

1. INTRODUCTION

Quenching and partitioning (Q&P) steels yield an excellent balance of high tensile strength and good elongation with similar chemical compositions as conventional TRIP steels [1-3]. They are produced via the Q&P process which consists of a quenching and a following partitioning step. During the quenching step, fully austenitized or intercritically annealed steels are quenched to temperatures (hereafter referred to as 'quench temperature') below the martensite start (Ms) temperature but above the martensite finish (Mf) temperature in order to form a controlled volume fraction of martensite. The quenched steels are then held at the same or higher temperatures than the quench temperature during the subsequent partitioning step. Austenite that prevails after quenching is considered to be stabilized through carbon partitioning from martensite into the austenite during the partitioning treatment.

It has been suggested that the carbon partitioning from martensite into austenite is controlled by the constrained carbon equilibrium (CCE) criterion [4]. This criterion aims at predicting the carbon concentration in austenite under the condition where (I) competing reactions, such as cementite or transition carbide formation, bainite transformation, etc., are suppressed; (II) an identical carbon chemical potential exists in both ferrite (or martensite) and austenite; and (III) the carbon partitioning proceeds under the assumption that the interface between ferrite and austenite does not migrate.

However, competing reactions such as bainite transformation [5-8] and carbide precipitation in martensite [8,9] have repeatedly been observed in the Q&P process. The bainite transformation can also contribute to carbon enrichment into the remaining austenite if carbide precipitation is suppressed by the addition of Si. If carbide precipitates in martensite, some of the carbon is consumed to form the carbide, reducing the remaining amount of carbon in martensite that can be enriched in austenite during partitioning. Hence, the austenite carbon concentration after the partitioning step in this case is presumed

* Corresponding author. E-mail: y-toji@jfe-steel.co.jp, telephone: +81 43 262 2906.

to be lower than that predicted under the CCE conditions excluding carbide precipitation. Therefore, this study aims to reveal the complicated competing phenomena by separating each of them.

2. EXPERIMENTAL PROCEDURE

The Q&P process has mainly been applied to steels with similar chemical compositions as conventional TRIP steels [1,5]. In such steels, bainite formation is practically unavoidable [5] as the chemical compositions are designed to promote bainite formation during austempering in the same temperature range as the partitioning step. This makes it difficult to distinguish the contributions to carbon enrichment into austenite during the partitioning step caused by the bainite transformation from that caused by the carbon partitioning from martensite. For separating carbon partitioning between martensite and austenite from bainite transformation, a chemical composition with Ms and Mf temperatures, respectively, above and below room temperature was selected. Fig. 1 shows the comparison between (a) the heat treatment applied in this study and (b) a general Q&P heat treatment. The bottom figures schematically show the relationship between partitioning time and retained austenite (γ) volume fraction as measured by, for example, X-ray diffraction (XRD) at room temperature after cooling from the partitioning temperature (PT). In the case of the general Q&P heat treatment (Fig. 1(b)), the remaining austenite at the quench temperature (QT) is unstable at room temperature so that the retained austenite volume fraction before partitioning treatment, which is measured at room temperature, is almost zero. Therefore, the exact amount of austenite remaining at the quench temperature can generally not be measured and hence has to be estimated, for instance, by using the Koistinen-Marburger equation [10]. The remaining austenite at the quench temperature is stabilized through the carbon partitioning from martensite and/or the bainite transformation. The austenite volume fraction measured at room temperature increases with the stabilization process, regardless of whether austenite decomposition occurs (indicated by case (4)) or not (indicated by case (3)). Even if the volume fraction becomes stable for longer partitioning times such as indicated by case (3), the value cannot be compared with the exact initial austenite fraction (γ_0) due to the reason mentioned above. Therefore, the austenite volume fraction measured at room temperature does typically not enable one to decide whether austenite decomposition occurs or not during the partitioning treatment. In contrast, in the heat treatment applied in this study (Fig. 1(a)), the remaining austenite after the first quenching is stable at room temperature

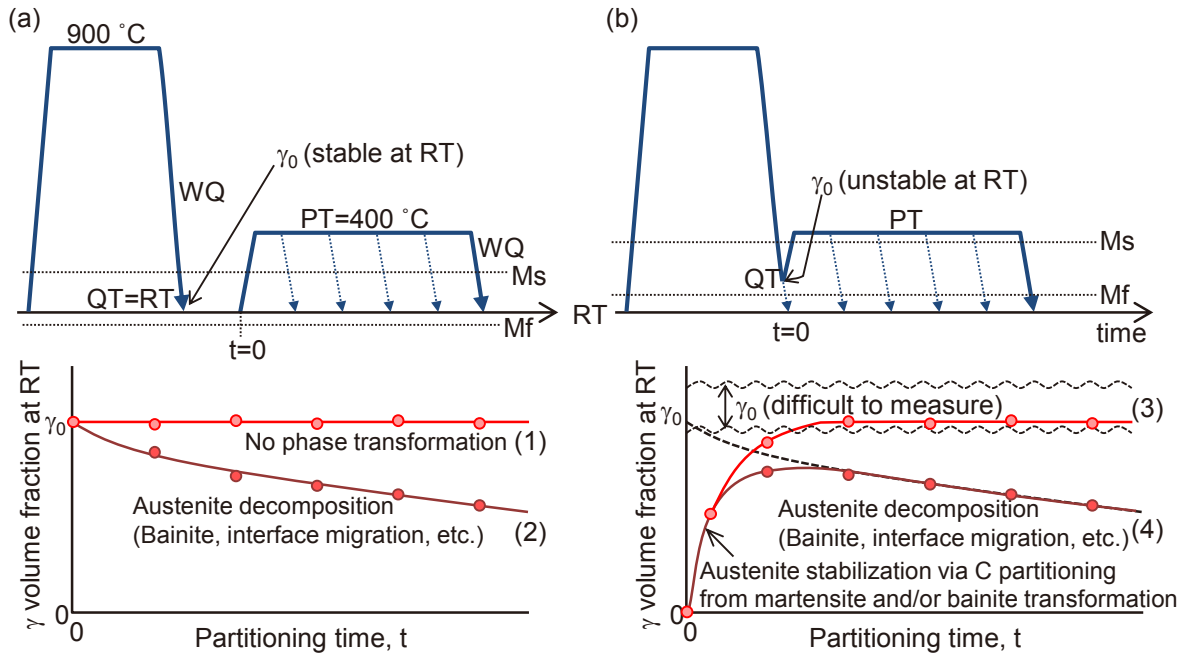

Fig. 1. Comparison between (a) the heat treatment applied in this study and (b) a general Q&P heat treatment. The bottom figures schematically show the relationship between partitioning time and retained austenite (γ) volume fraction as measured by, for instance, X-ray diffraction at room temperature after cooling from PT. RT: room temperature, QT: quench temperature, PT: partitioning temperature, Ms: martensite start temperature, Mf: martensite finish temperature, WQ: water quenching, γ_0: austenite volume fraction at QT.

(without the partitioning step) and, hence, its volume fraction can be quantified. It should be noted that the stability of the remaining austenite should not decline during the partitioning step since its carbon concentration dose not decrease during the partitioning step unless carbide precipitation occurs in austenite, which can be suppressed by Si. If austenite decomposition occurs during the partitioning step, the volume fraction of austenite must decrease. Therefore, it can be concluded from the austenite volume fraction change measured at room temperature whether austenite decomposition occurs (indicated by case (2)) or not (indicated by case (1)), during the partitioning process. The actual chemical composition was Fe-0.59wt%C(2.7at%C)-2.0wt%Si-2.9wt%Mn. The carbon content in this model alloy was higher than that in typical alloys to which Q&P process have been applied [1,5] in order to lower the Mf temperature below room temperature. The high amount of Si (2.0 wt.%) was added to suppress carbide formation. The steel was prepared by vacuum induction melting. The ingot was homogenized at 1240 ˚C for 48 h, then air cooled to room temperature. The homogenized ingot was reheated and held at 1200 ˚C for 30 min followed by hot rolling to a sheet with a thickness of 3.6 mm, then air cooled to room temperature. The hot rolled steel sheet were then heat-treated according to Fig. 1(a). They were austenitized at 900 ˚C for 3 min, then water quenched, followed by a partitioning step at 400 ˚C for 10-3000 s in a salt bath furnace. The specimens before and after the partitioning step are hereafter referred to as 'as-quenched specimen' and 'partitioned specimen', respectively.

To investigate the carbon partitioning behavior from martensite into austenite accompanied by carbide precipitation inside the martensite, Fe-1.07wt%C-2.2wt%Si-2.9wt%Mn (Steel A) and Fe-0.59wt%C-2.0wt%Si-2.9wt%Mn (Steel B) were used. The carbon contents in these model alloys were higher than that in typical alloys used for Q&P processing [1,5] in order to lower the Mf temperature below room temperature. For these alloys, the room temperature or even lower temperatures can be used as quench temperature, which enables us to directly observe the initial microstructure and atomic distribution before partitioning step. The hot rolled steel sheet prepared under the same conditions as described above was austenitized at 900 ˚C for 3 min, then quenched in water with a temperature of 30~17 ˚C, followed by a partitioning step at 400 ˚C for 300 s in a salt bath furnace. Some specimens cut from steel A quenched in 17 ˚C water were further quenched to -20 ˚C or -63 ˚C prior to the partitioning step to vary the martensite volume fraction. The specimens before and after the partitioning step are hereafter referred to as 'as-quenched specimen' and 'partitioned specimen', respectively.

The amount of retained austenite was quantified by X-ray diffraction (XRD) with Co Kα radiation. Microstructures in the cross section perpendicular to the transverse direction (TD cross section) etched with 0.1~0.3% Nital were observed by optical microscopy and scanning electron microscopy (SEM). Electron back scatter diffraction (EBSD) measurement was performed with a step size of 50 nm to distinguish austenite from martensite. Carbon partitioning between martensite and austenite was investigated by using a field-emission electron probe micro analyzer (FE-EPMA). The use of a FE-type electron emitter can achieve a narrower emission area as compared to the conventional W or LaB6-type electron emitter. Also, a relatively low voltage of 6 kV was used to minimize the excitation volume. A probe current of 70 nA was used. The carbon concentration was determined using a standard calibration curve, which was obtained using seven standard specimens in the range of 0.0083~1.07 wt.%C. Standard deviations were below 0.021 wt.%. In the FE-EPMA measurements, the line-analysis mode was used to obtain carbon profiles across regions of interest. The detection time for each point was 2 s in single-scan mode. Atom probe tomography (APT) was also applied for the near-atomic quantitative investigation of carbon partitioning. Samples for APT measurements were prepared using focused ion beam (FIB) milling. APT analyses were performed using a local electrode atom probe (LEAP 3000X HR) in the voltage mode at a specimen temperature of around 65 K. Data analyses were performed using the IVAS software.

3. RESULTS AND DISCUSSION

3.1. Carbon partitioning from martensite into austenite precluding bainite transformation [11]

Fig. 2 shows the austenite volume fraction of the as-quenched and partitioned specimens of Fe-0.59wt%C-2.0wt%Si-2.9wt%Mn heat treated as Fig. 1(a) measured by XRD at room temperature. Approximately 8 vol% of austenite exists in the as-quenched specimen, which means that the Mf temperature of the steel is indeed below room temperature. The austenite volume fraction in the specimens does not change by partitioning up to 3000 s. This indicates that austenite decomposition, i.e.

bainite transformation, did not occur under the partitioning conditions in this study. Fig. 3(a) shows SEM microstructure of the specimen partitioned at 400 ˚C for 300 s. Many plate-shaped precipitates with white contrast are observed, which are considered to be carbides. From the comparison between the SEM image and the phase map obtained by EBSD (Fig. 3(b)), the relatively large flat grains with white contrast in the SEM image can be recognized as retained austenite. The retained austenite appears to exist on prior austenite grain boundaries, packet boundaries, and block boundaries. Although thin film-like austenite layers between martensite laths are also expected, they are barely visible due to the limited resolution of EBSD.

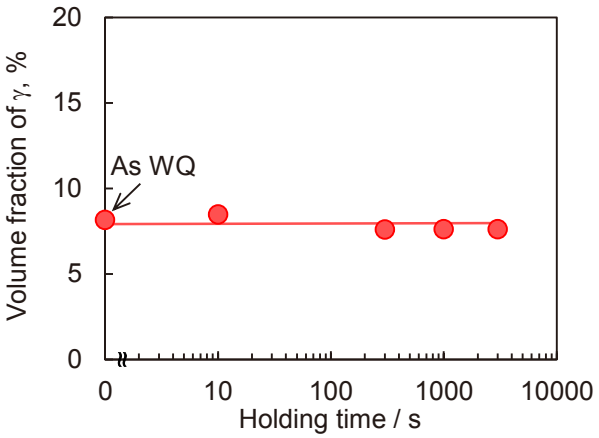

Fig. 2 Change in austenite volume fraction during partitioning at 400 ˚C obtained by XRD. γ: austenite, WQ: water quenching.

Figs. 4(a) and 4(c) show atom maps of C and Mn of the as-quenched specimen and concentration profiles along the black arrow indicated in the C atom map. Although Mn are distributed uniformly, the carbon concentration fluctuates in the range between 1.5 at% and 4.5 at% in the as-quenched state. However, no regions that are regarded as austenite were found in any of the eight APT samples taken from the as-quenched specimen, which were seen in the partitioned specimens shown later. This means that the carbon partitioning from martensite to austenite during water quenching and sample storage at room temperature was essentially negligible. The average carbon concentration in these eight as-quenched samples analyzed by APT was 2.77 at%, which is in good agreement with the bulk carbon content of the steel (2.7 at%). Fig. 4(b) shows atom maps of C and Mn of the specimen partitioned at 400 ˚C for 300 s, where iso-concentration surfaces representing 2.7 at% C are displayed in yellow. C, Mn proxigrams across 5 at% carbon iso-concentration surface created inside the cylinder in Fig. 4(b) are shown in Fig. 4(d). Clear carbon enrichment in austenite was observed and the carbon concentration inside this region was 6-10 at%. Mn also slightly partitions between martensite and austenite under this conditions. The change in carbon concentration in austenite during partitioning at 400 ˚C analyzed by APT is shown in Fig. 5. The austenite carbon concentrations are the analyzed values in the austenite regions at least 2 nm away from the interface between martensite and austenite in order to exclude the influence of the artifact around the interface. The austenite carbon concentration rapidly increased with partitioning for 10 s and then gradually increased upon further partitioning. These results quantitatively reveal carbon partitioning from martensite into austenite in the absence of influences by bainite transformation.

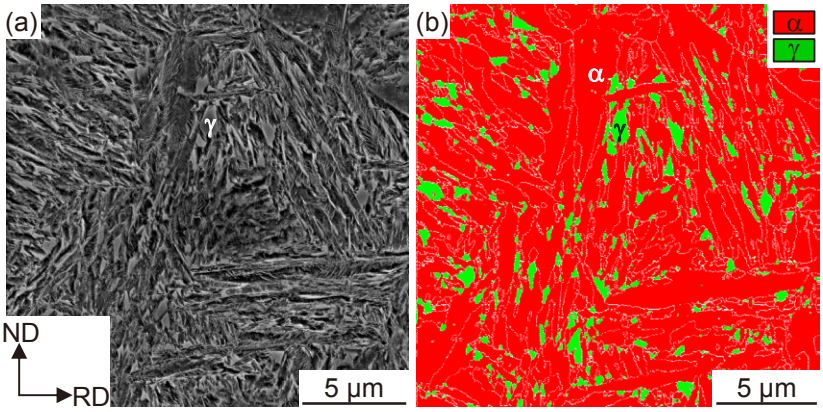

Fig. 3. Comparison between SEM image (a) and phase map (b) obtained by EBSD of the specimen partitioned at 400 ˚C for 300 s. White lines in (b) represent high angle boundaries (15˚-180˚).

The experimentally observed carbon partitioning behavior is compared to the CCE theory proposed by Speer et al. [4]. The carbon concentrations in each phase under the CCE conditions were calculated by Thermo-Calc using the data base TCFE6. The calculated austenite carbon concentration in the present case was 19.9 at% (5.05 wt%). The experimental value (Fig. 5) is much lower than the calculated austenite carbon concentration under the CCE conditions. The main reason for this discrepancy is considered to be the carbide precipitation inside the martensite during partitioning as shown in Fig. 3,

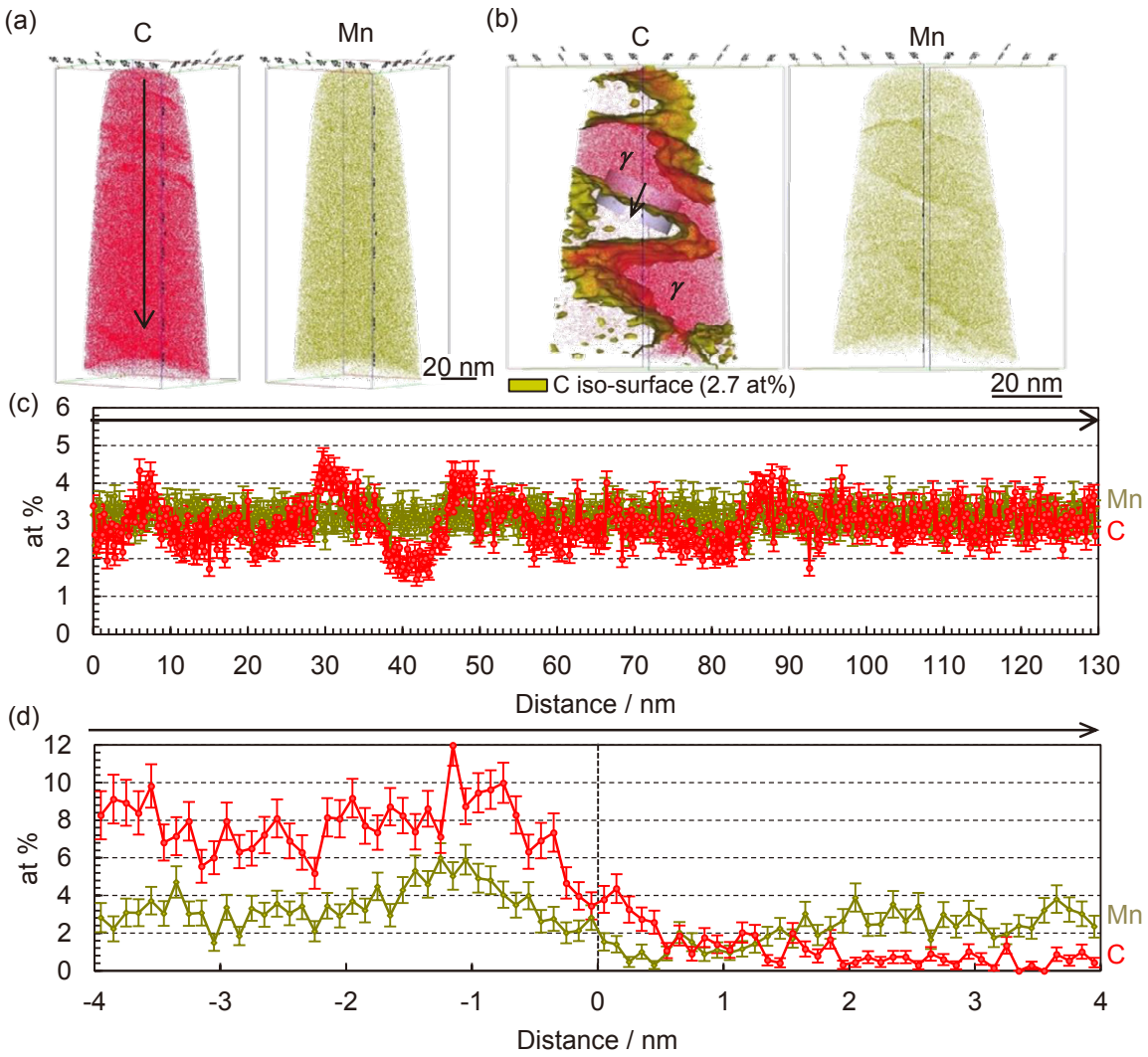

Fig. 4. Atom maps of C and Mn of (a) as-quenched specimen and (b) specimen partitioned at 400 ˚C for 300 s. (c)(d) Concentration profiles of C and Mn along the black arrow indicated in the C atom map in (a) and (b), respectively. The error bars in (c) and (d) represent the one-sigma statistical error.

regardless of the high Si content. Kozeschnik et al. [12] reported that Si strongly suppresses carbide precipitation in austenite, but is less effective in ferrite (or martensite) because the driving force for the precipitation is too high due to the low solubility of carbon in ferrite. Especially in the case of the present steel in which the carbon content is high, carbide precipitation in martensite is considered to be practically unavoidable. Therefore, predictions that include carbide precipitation are also needed in order to achieve a more precise estimate of the carbon concentration in austenite after the Q&P heat treatment, which will be discussed in the next section.

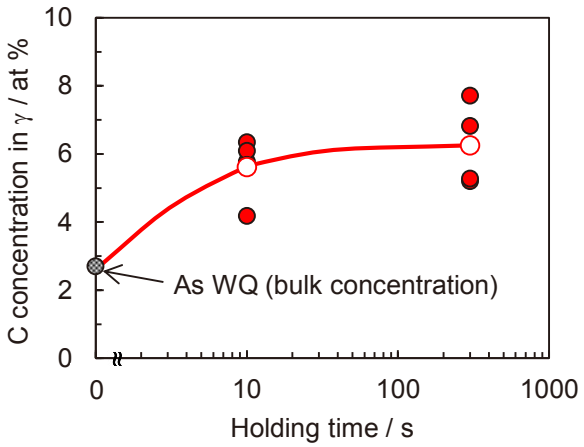

Fig. 5. Change in C concentration in γ during partitioning at 400 ˚C. Solid symbols show the individual C concentrations obtained from the APT results. Open symbols show the average C concentration of the measured values at each partitioning time.

3.2 Carbon partitioning accompanied by carbide precipitation [13]

As mentioned in the previous section, adequate models are required that include carbide precipitation during the partitioning step, hence providing a more precise estimate of the carbon concentration in austenite after the Q&P heat treatment. There is, however, currently no model dealing with the carbon partitioning behavior from martensite into austenite under conditions that carbide precipitation occurs in martensite during the partitioning step. In this section, we conducted an experimental analysis of the carbon partitioning behavior from martensite into austenite accompanied by carbide precipitation inside the martensite during a partitioning step. A modified CCE model is introduced to explain the experimental results.

Fig. 6 shows optical and SEM micrographs of steel A (1.07wt%C) quenched to (a)(b) 17 ˚C and (c)(d) -63 ˚C, respectively, followed by a partitioning step at 400 ˚C for 300 s. The dark regions in optical micrographs are martensite which forms during quenching and the white regions are austenite. The volume fraction of martensite increased with decreasing the quench temperature, namely, 15% (quenched to 30˚C), 22% (quenched to 17˚C), 52% (quenched to -20˚C) and 75% (quenched to -63˚C), respectively. In the SEM images, a considerable amount of carbide (white contrast) can be observed inside the martensite. It was confirmed by XRD that the austenite volume fraction of specimens did not change during holding at 400 ˚C. This indicates that austenite decomposition, i.e. bainite transformation, did not occur under the partitioning conditions in this study.

Carbon partitioning during the partitioning step in the specimens with different martensite volume fraction was investigated by means of FE-EPMA. At first, the carbon distributions in the specimens as-quenched to different temperatures were confirmed to be practically uniform, irrespective of the martensite volume fraction. This indicates that the carbon partitioning from martensite to austenite during quenching to each of these temperatures was essentially negligible, which is in line with the result obtained on steel B via APT (Fig. 4). Fig. 7 shows FE-EPMA carbon profile of the specimen quenched to 17 ˚C, followed by partitioning at 400 ˚C for 300 s. The white line in the upper SEM image indicates the probed line. The carbon distribution in these partitioned specimen is obviously inhomogeneous. Clear pileup of carbon around the martensite/austenite (M/A) interface inside the austenite region can be observed (blue arrows in Fig. 7(b)). This indicates that some carbon atoms could partition from the martensite into the austenite during the partitioning step at 400 ˚C, even though a considerable amount of carbide formed inside the martensite. The austenite carbon concentration in the

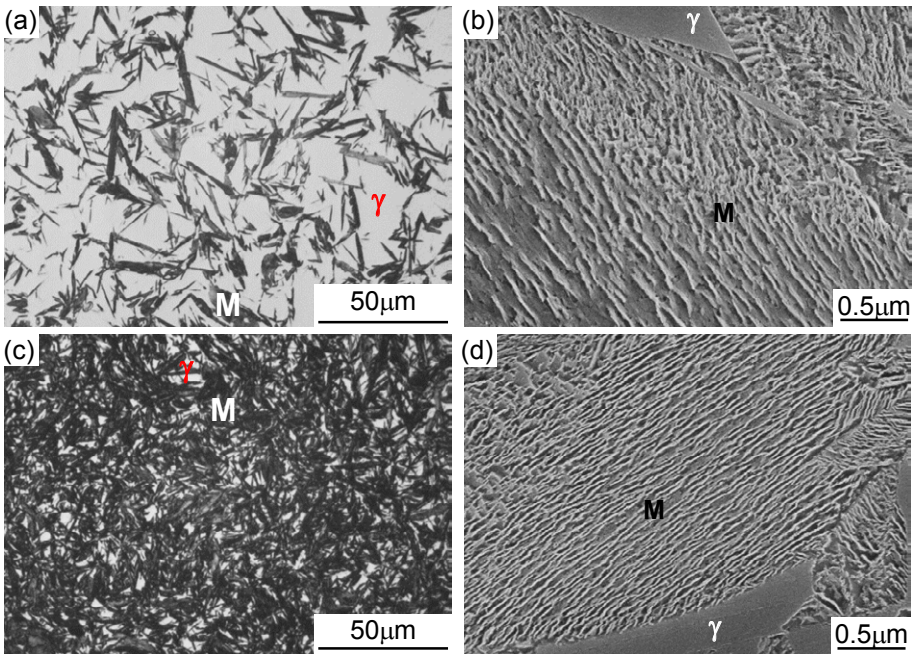

Fig. 6. Optical (a)(c) and SEM (b)(d) micrographs of steel A (1.07wt%C) quenched to (a)(b) 17 ˚C and (c)(d) -63 ˚C, followed by partitioning at 400 ˚C for 300 s. γ: austenite, M: martensite.

specimens partitioned at 400 ˚C for 300 s obtained by FE-EPMA is summarized in Fig. 8 as a function of the martensite volume fraction. Although the carbon concentration was not homogeneous in the austenite after partitioning for 300 s as shown in Fig. 7, the austenite carbon concentration in the vicinity of the M/A interface is the most important information to understand the equilibrium conditions across the interface. Therefore, the range of the austenite carbon concentration values in the vicinity of the M/A interfaces are shown as red bars in Fig. 8. In either specimen with their different martensite fraction, the austenite carbon concentrations are higher than the bulk carbon content (1.07 wt%). The most important finding here is that the austenite carbon concentration near the interface in these specimens with different martensite volume fraction is nearly the same. This indicates that the carbon partitioning behavior is not influenced by the volume fraction of pre-existing martensite.

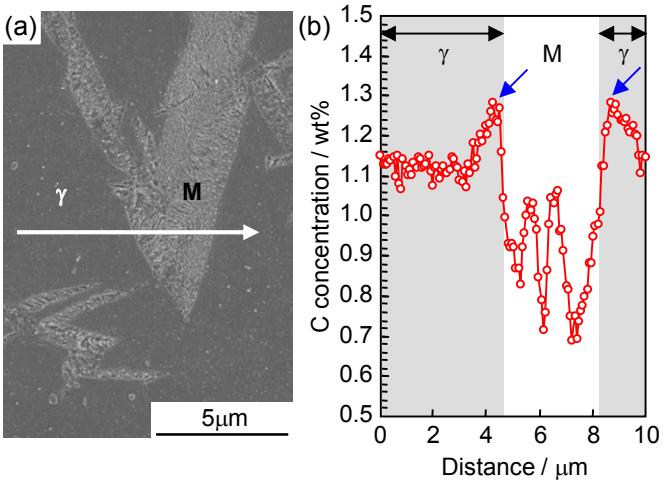

Fig. 7. (a) SEM microstructure of steel A (1.07wt%C) quenched to 17 ˚C followed by partitioning at 400 ˚C. (b) Carbon concentration profile along the white arrow in (a) obtained by FE-EPMA. γ: austenite, M: martensite.

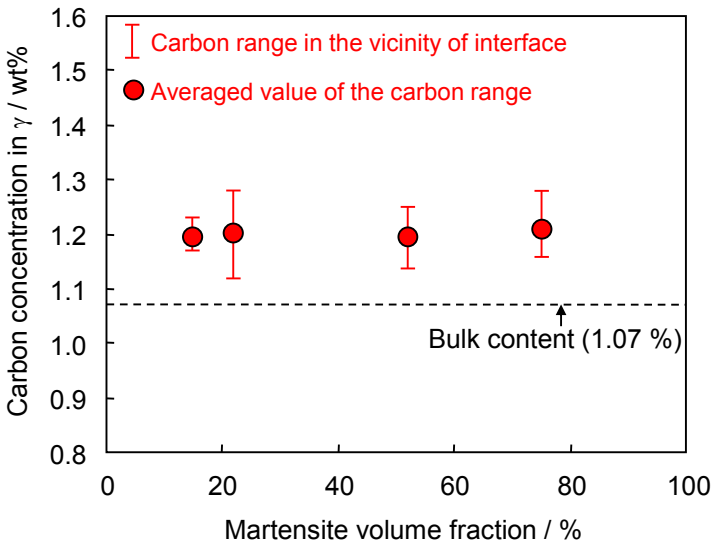

Fig. 8. Influence of martensite volume fraction on austenite carbon concentration in steel A (1.07wt%C) quenched to 30 ~ -63 ˚C followed by partitioning at 400 ˚C for 300 s. γ: austenite.

In order to understand the influence of the bulk carbon concentration on carbon partitioning behavior, carbon partitioning in the lower carbon steel (steel B, 0.59wt%C) quenched to room temperature followed by partitioning at 400 ˚C for 300 s was also investigated. For this specimen, atom probe tomography was applied since the spatial resolution of FE-EPMA is not fine enough relative to the size of the austenite regions in this specimen (Fig. 3). The averaged carbon concentration obtained from the austenite regions in 5 atom probe samples were 1.41 wt% (6.11 at%). This value is similar or rather slightly higher than the austenite carbon concentrations observed in the 1.07 wt%C steel (steel A) shown in Fig. 8, even though the bulk carbon concentration of steel B is lower than that of steel A.

The experimentally observed carbon partitioning behavior is compared to the CCE model proposed by Speer et al. [4] and a modified CCE model for understanding the carbon partitioning behavior in the case where carbide precipitation occurs in martensite. The modified CCE model, hereafter referred to as CCEθ (Constrained Carbon Equilibrium accompanied by θ precipitation) is schematically drawn in Fig. 9, together with the original CCE model. Fe-X on the left hand side of the abscissa axis refers to iron (Fe) with other substitutional elements (X) included in alloys. The atomic fraction of substitutional elements such as Si, Mn, etc. is constant in these diagrams. In the original CCE model, carbide precipitation is not taken into account, i.e. only carbon partitioning between martensite (ferrite) and austenite is considered. In the model we propose here, the free energy of the cementite is also drawn (Fig. 9(b)). Since the cementite precipitates inside the martensite, the carbon potential in the ferrite and cementite in the martensite should be identical. In addition, the carbon potential in the austenite should

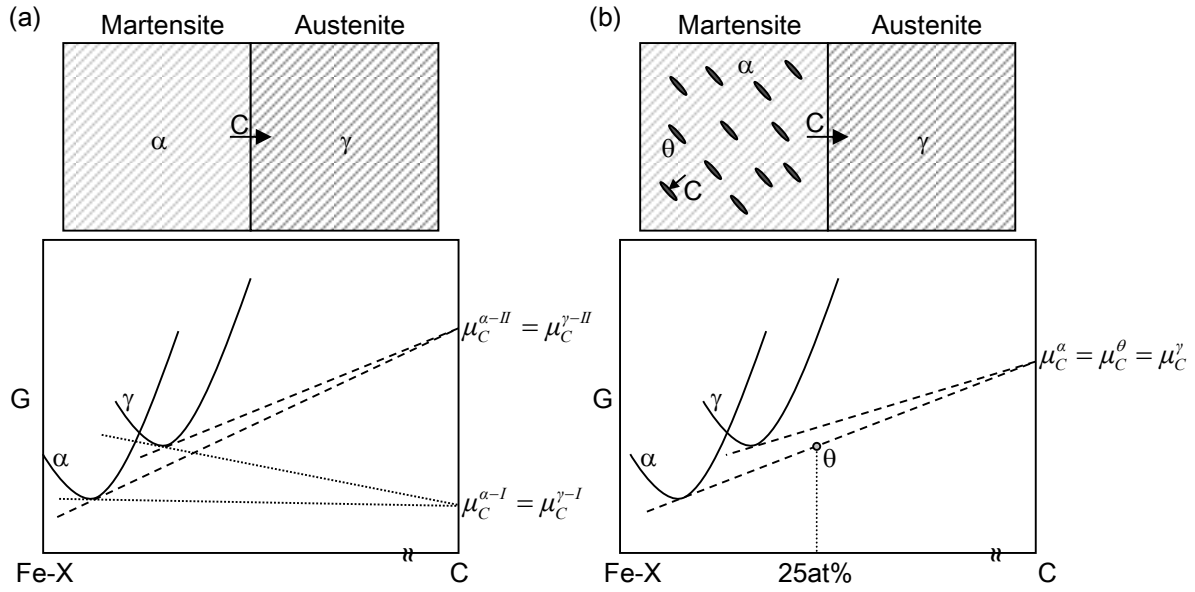

Fig. 9. Comparison between (a) original CCE model and (b) modified CCE model. α: ferrite, γ: austenite, θ: cementite, C: carbon, Fe: iron, X: substitutional elements, $\mu_C^{\alpha}, \mu_C^{\gamma}, \mu_C^{\theta}$: carbon potential in ferrite, austenite, cementite, respectively.

be the same as that in ferrite, which is satisfied by drawing a tangent to the austenite free energy curve from the point where the tangent to the ferrite free energy curve intersects the carbon axis (right axis). This condition is expressed by the following equations:

$$3\mu^{\alpha}_{Fe_{CCE\theta}} + \mu^{\alpha}_{C_{CCE\theta}} = G(Fe_3C) \quad \cdots(1)$$

$$\mu^{\alpha}_{C_{CCE\theta}} = \mu^{\gamma}_{C_{CCE\theta}} \quad \cdots(2)$$

where $\mu^{\alpha}_{Fe_{CCE\theta}}$ is the chemical potential of iron in ferrite, $\mu^{\alpha}_{C_{CCE\theta}}$ and $\mu^{\gamma}_{C_{CCE\theta}}$ are the chemical potentials of carbon in ferrite and austenite under CCEθ conditions, respectively. $G(Fe_3C)$ is the Gibbs free energy of cementite. Eq. 1 expresses the tangent to the ferrite free energy curve passing the point of the cementite free energy. These conditions are coupled with the condition that the interface between ferrite and austenite does not migrate, which is expressed as the following form:

$$f^{\gamma}_{CCE\theta}(1 - X^{\gamma}_{C_{CCE\theta}}) = f^{\gamma}_{i}(1 - X^{alloy}_{C}) \quad \cdots(3)$$

where f^{γ}_{i} and $f^{\gamma}_{CCE\theta}$ represent the initial austenite mole fraction before the partitioning step and the austenite mole fraction under CCEθ conditions, respectively. X^{alloy}_{C} and $X^{\gamma}_{C_{CCE\theta}}$ represent the bulk carbon concentration, and the carbon concentration in the austenite under CCEθ conditions, respectively. This equation means that the atomic fractions of the substitutional elements in the austenite do not change during the partitioning step. The following two more equations are required to describe the carbon equilibria.

$$f^{\alpha}_{CCE\theta}X^{\alpha}_{C_{CCE\theta}} + f^{\gamma}_{CCE\theta}X^{\gamma}_{C_{CCE\theta}} + f^{\theta}_{CCE\theta}X^{\theta}_{C_{CCE\theta}} = X^{alloy}_{C} \quad \cdots(4)$$

$$f^{\alpha}_{CCE\theta} + f^{\gamma}_{CCE\theta} + f^{\theta}_{CCE\theta} = 1 \quad \cdots(5)$$

where $f^{\alpha}_{CCE\theta}$ and $f^{\theta}_{CCE\theta}$ represent the ferrite and cementite mole fractions under CCEθ conditions, respectively. $X^{\alpha}_{C_{CCE\theta}}$ and $X^{\theta}_{C_{CCE\theta}}$ represent the carbon concentrations in ferrite and cementite under CCEθ conditions, respectively ($X^{\theta}_{C_{CCE\theta}}$ = 0.25). Eq. 4 expresses the mass balance of carbon. Eq. 5 describes the relationship among the phase fractions. The situation expressed by Fig. 9 and Eqs. 1 to 5 is that: (I) the ferrite and cementite are under para equilibrium conditions and (II) the ferrite (which contains cementite) and the abutting austenite are under CCE conditions. This means that the austenite volume fraction does practically not change, while the ferrite volume fraction changes accompanied by the cementite precipitation. In reality the austenite volume fraction should of course change slightly as the atomic fraction of carbon inside the austenite increases during the partitioning step.

An essential difference between the CCE and CCEθ models is the influence of the initial austenite volume fraction and the carbon content before the partitioning step on the resultant austenite carbon concentration after partitioning. Under CCE conditions at a specific partitioning temperature, there is an infinite set of carbon concentrations in ferrite and austenite having equal carbon potentials as shown in Fig. 9(a). Hence the initial austenite fraction and carbon content is required to select one of them. In other words, the austenite carbon concentration changes with the initial austenite fraction and carbon content. On the other hand, it is expected that the austenite carbon concentration is uniquely identified only by the thermodynamic conditions as shown in Fig. 9(b) under CCEθ conditions, independent of the initial austenite volume fraction and carbon content if the contents of other alloying elements such as Si and Mn in the alloys are the same. In this case, the volume fraction of carbide inside the martensite would change as a function of the initial martensite fraction and bulk carbon content so as to provide the required carbon atoms to maintain the identical austenite carbon concentration.

Fig. 10 shows the experimentally obtained carbon concentrations in austenite together with the values predicted by the CCE model. Regarding the experimental data, the austenite carbon concentrations in the 1.07 wt%C steel (steel A) with a martensite volume fraction of 15~75% and those in the 0.59 wt%C steel (steel B) with 92 vol% martensite are plotted together. The range of the austenite carbon concentration values in the vicinity of the M/A interface and their averaged values are shown in this figure. As mentioned before, the martensite volume fraction has essentially no influence on the experimentally obtained austenite carbon concentrations in steel A. In addition to that, the austenite carbon concentration in steel B is also nearly the same as those in steel A, although that in steel B is slightly higher than those in steel A. Therefore, we conclude that the austenite carbon concentration in the vicinity of the interface was neither influenced by the martensite volume faction nor by the bulk carbon concentration of the alloys. The austenite carbon concentration calculated by the CCE model in the same way as described in 2.3 is drawn as the red and blue solid lines for steel A and steel B, respectively. According to the CCE model, the carbon concentration in austenite is predicted to increase with increasing martensite volume fraction and bulk carbon content. Therefore, more carbon can accumulate inside the austenite if the martensite volume fraction is larger and the austenite volume fraction is smaller. Regarding the influence of the bulk carbon content, more carbon can enrich in austenite in steels with higher bulk carbon content as compared to the steels with lower bulk carbon content having same martensite volume fraction. This tendency predicted by the CCE model is, however, inconsistent with the experimental results obtained in the present study with different martensite volume fractions and bulk carbon contents under the conditions that carbide precipitates in martensite. This deviation is attributed to the carbide precipitation inside the martensite as observed in this study (Fig. 6), which is not considered in the CCE model. Carbide precipitation consumes some of the carbon, thus its partitioning into austenite is reduced. The austenite carbon concentrations as predicted by the CCEθ model are added as green line in Fig. 10. The free energies of austenite, ferrite and cementite at 400 ˚C were calculated by Thermo-Calc using the data base TCFE6. The free energy of cementite was calculated using the actual chemical composition in cementite of the specimen held

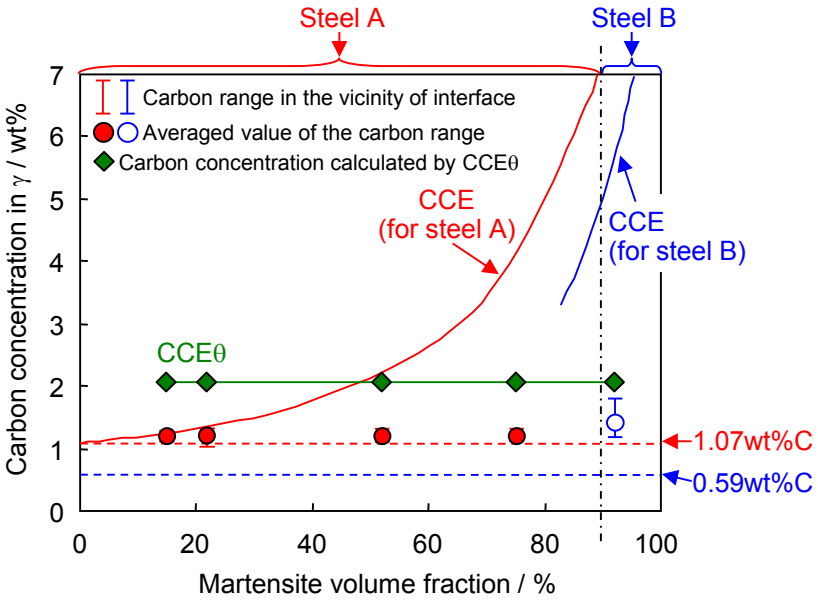

Fig. 10. Comparison between the experimentally obtained carbon concentrations in austenite and that predicted by CCEθ (constrained carbon equilibrium accompanied by θ precipitation) model assuming Si partitioning between θ and surrounding ferrite at 400 ˚C for 300 s. Carbon concentrations in austenite predicted by CCE for steel A and steel B are also drawn.

at 400 ˚C for 300s measured by APT [13]. According to the CCEθ prediction, the austenite carbon concentration is neither influenced by the initial austenite volume fraction nor by the nominal carbon content as mentioned above. Therefore, the green line is horizontal regardless of the martensite volume fraction and the bulk carbon content. This is consistent with the trend observed in the experimental results, which supports the applicability of the CCEθ model for predicting the carbon concentration in austenite in cases when carbides precipitate inside the martensite. However, the calculated carbon concentration by CCEθ was rather higher than the experimental values. This can probably be attributed to the fact that the free energy of cementite is not entirely correct. The free energy of cementite is affected by elemental partitioning between ferrite and cementite. It is hence necessary to consider the free energy change in the corresponding carbides at each partitioning time step for predicting the austenite carbon concentration accurately. The free energies of cementite in multi component systems are not yet fully understood and first-principal studies are being pursued along these lines [14,15].

4. SUMMARY

Carbon partitioning from martensite to austenite during the partitioning step in a Q&P heat treatment excluding any interfering effects from the bainite transformation was quantitatively revealed at the atomic scale by APT using 0.59 wt% carbon steel. Carbon partitioning behavior from martensite into austenite accompanied by the carbide precipitation inside the martensite was investigated by means of FE-EPMA and APT using 1.07 wt% and 0.59 wt% carbon steels with various martensite volume fractions. A modified prediction model for the austenite carbon concentration after the partitioning step in the Q&P process, which can be applied to the case where carbide precipitation occurs in martensite, was proposed to explain the experimental results. The austenite carbon concentration predicted by the modified model showed the same trend as the experimental results, i.e. it was independent of the martensite volume fraction and of the bulk carbon content. The predicted carbon value was closer to the experimental value than that predicted by the original CCE model.

REFERENCES

[1] J.G. Speer, A.M. Streicher, D.K. Matlock, F.C. Rizzo, G. Krauss: Austenite formation and decomposition, E.B. Damm, M. Merwin (Eds.), TMS/ISS, Warrendale, 2003, 505-522.
[2] B.C. De Cooman, J.G. Speer: Steel Res. Int., 77(2006), 634-640.
[3] E. De Moor, J.G. Speer, D.K. Matlock, J.H. Kwak, S.B. Lee: Steel Res. Int., 83(2012), 322-327.
[4] J.G. Speer, D.K. Matlock, B.C. De Cooman, J.G. Schroth: Acta Mater., 51(2003), 2611-2622.
[5] M.J. Santofimia, T. Nguyen-Minh, L. Zhao, R. Petrov, I. Sabirov, J. Sietsma: Mater. Sci. Eng. A, 527(2010), 6429-6439.
[6] M.J. Santofimia, L. Zhao, R. Petrov, C. Kwakernaak, W.G. Sloof, J. Sietsma: Acta Mater., 59(2011), 6059-6068.
[7] K. Seto, H. Matsuda: Mater. Sci. Technol., 29(2013), 1158-1165.
[8] M.J. Santofimia, L. Zhao, J. Sietsma: Metall. Mater. Trans. A, 40(2009), 46-57.
[9] D.V. Edmonds, K. He, F.C. Rizzo, B.C. De Cooman, D.K. Matlock, J.G Speer: Mater. Sci. Eng. A, 438-440(2006), 25-34.
[10] D.P. Koistinen, R.E. Marburger: Acta Metall., 7(1959), 59-60.
[11] Y. Toji, H. Matsuda, M. Herbig, P.P. Choi, D. Raabe: Acta Mater., 65(2014), 215-228.
[12] E. Kozeschnik, H.K.D.H. Bhadeshia: Mater. Sci. Technol., 24(2008), 343-347.
[13] Y. Toji, G. Miyamoto, D. Raabe: Acta Mater., 86(2015), 137-147.
[14] B. Hallstedt, D. Djurovic, J. Appen, R. Dronskowski, A. Dick, F. Körmann, T. Hickel, J. Neugebauer: CALPHAD, 34(2010), 129-133.
[15] K.C. Ande, M.H.F. Sluiter: Acta Mater., 58(2010), 6276-6281.